Microchemical Journal 203 (2024) 110919



Contents lists available at ScienceDirect

Microchemical Journal

journal homepage: www.elsevier.com/locate/microc





Evaluation of enzyme-mimetic nanoparticle employed lateral flow immunoassay device for breast cancer diagnosis by detecting thioredoxin 1 in actual human serum

J.C. Shin [a], D.W. Kim [a], S.H. Kim [a], X. Yang [a], Y.G. Kim [b], E.A. Kang [b], J.A. Song [a,*], K.H. Suh [a]

[a] E&S Healthcare, Daejeon, Republic of Korea
[b] Nature Inspired Energy Technology (NIET), Daejeon, Republic of Korea

ARTICLE INFO

Keywords:
Breast Cancer
Biomarker
Thioredoxin 1
Lateral flow immunoassay
Enzyme-Mimetic Nanoparticles
In-vitro diagnostic medical device

ABSTRACT

Breast cancer, despite its high incidence, exhibits significantly improved survival rates when diagnosed at an early stage. Consequently, rapid and accurate diagnosis is crucial for managing breast cancer. In this paper, we present the development of a lateral flow immunoassay device for the swift diagnosis of breast cancer by detecting thioredoxin 1, a novel biomarker for early breast cancer detection. To improve the sensitivity of the device, we utilized the enzyme mimetic nanoparticle, H-Pt-Nanozyme, as a detection label, potentially allowing signal amplification through enzyme reactions. Adjusting the detection range for breast cancer qualitative diagnosis based on the previously proposed cut-off value of 11.4 ng/mL, the optimized device demonstrated similar sensitivity and superior reproducibility compared to device using gold nanoparticles, a commonly used detection label, under the same conditions. The developed device successfully differentiated between 10 breast cancer patients and 10 healthy individuals by naked-eye detection. Finally, to prevent false-negative diagnosis, we confirmed the feasibility for signal amplification through the utilization of enzyme reactions. The device developed in this study allows for the effective discrimination of early-stage breast cancer patients, reducing false-negative rates associated with mammography and ultrasonography, the current gold-standard diagnostic methods according to breast cancer diagnosis and screening guidelines. Additionally, its potential to assist in clinical suspicion in clinical settings raises expectations for preventing unnecessary surgeries in false-positive cases.

1. Introduction

Breast cancer (BC) is a rapidly increasing global health concern [1,2]. According to the Global Cancer Statistics 2020: GLOBOCAN report, approximately 2.26 million women were diagnosed with BC, accounting for 24.5 % of all female cancers worldwide. It ranked as the most prevalent cancer among women globally. During the same period, around 680,000 women succumbed to BC, constituting 15.5 % of all female cancer-related deaths and ranking as the leading cause of cancer deaths among women worldwide. While BC incidence is high in developed countries, the mortality rates are relatively elevated in less developed nations [3]. This trend is evident in the analysis of BC mortality trends conducted by the National Center for Health Statistics in the United States. The BC mortality rate in the U.S. has seen a reduction of approximately 43 % from 1989 to 2020 [4]. This decline is attributed to advancements in early detection and treatment through BC screening, underscoring the potential for reducing mortality rates when BC is detected early [5,6].

BC screening, as referred to here, targets women to detect BC early and accurately. Since it involves a large population, the screening

Abbreviations: BC, Breast Cancer; MMG, Mammography; WHO, World Health Organization; Trx1, Thioredoxin 1; ROS, Reactive Oxygen Species; ER, Estrogen Receptor; PR, Progesterone Receptor; ELISA, Enzyme-Linked Immunosorbent Assay; POCT, Point-of-Care Test; LFIA, Lateral Flow Immunoassay; H-Pt-NZ, H-Pt-Nanozyme; AuNPs, Gold Nanoparticles; CAb, Capture Antibody; DAb, Detection Antibody; PPB, Potassium Phosphate Buffer; RT, Room Temperature; RH, Relative Humidity; C line, Control line; T line, Test line; PBST, Tween 20 in PBS; AEC, 3-Amino-9-Ethylcarbazole; NaCl, Sodium Chloride; LOD, Limit of Detection; SD, standard deviation; NC, Negative Control; PC, Positive Control; GHTF, Global Harmonization Task Force; NCCN, National Comprehensive Cancer Network; BI-RADS, Breast Imaging-Reporting and Data System; DMMG, Diagnostic Mammography; US, Ultrasonography.

* Corresponding author at: R&D team 1, 42, Gukjegwahak 11-ro, Yuseong-gu, Daejeon 34002, Republic of Korea.
E-mail address: sja@ens-h.com (J.A. Song).

https://doi.org/10.1016/j.microc.2024.110919
Received 13 February 2024; Received in revised form 3 April 2024; Accepted 3 June 2024
Available online 4 June 2024
0026-265X/© 2024 The Authors. Published by Elsevier B.V. This is an open access article under the CC BY-NC-ND license (http://creativecommons.org/licenses/by-nc-nd/4.0/).

method should be simple, safe, and have minimal side effects [7]. One such BC early detection method that meets these criteria is mammography (MMG), a type of breast imaging [8]. The World Health Organization (WHO) recommends MMG and recently suggested lowering the starting age for routine screening from 50 to 40 years [9,10].

However, one drawback of MMG is its poor user-friendliness due to the application of strong pressure on the breast during examination, causing significant discomfort and anxiety for the examinee [11–14]. Furthermore, MMG exhibits reduced sensitivity and specificity for dense breast tissue, a common characteristic in young women, resulting in an elevated false-negative and false-positive rate [15–18].

Recent studies have reported a growing trend in utilizing biomarkers found in human-derived substances to complement the limitations of MMG for BC diagnosis [19,20]. One such protein biomarker gaining attention for effective BC diagnosis is thioredoxin 1 (Trx1) [21–24]. Trx1 is a representative redox-regulating protein with key molecular functions in cell signaling, defense against oxidative damage and stress, and serving as a major electron donor to reduce hydrogen peroxide (H_2O_2), a representative reactive oxygen species (ROS) [25]. Trx1 helps eliminate cellular toxicity caused by ROS [26].

BC cells experience increased oxidative stress due to abnormal metabolic processes and the presence of hormone receptors, such as estrogen receptor (ER) and progesterone receptor (PR) [27,28]. This imbalance in antioxidant mechanisms leads to the upregulation of Trx1 in cancer cells [29]. In this scenario, cancer cells bring the overexpression of the antioxidant protein Trx1 to mitigate oxidative stress, promoting the sustained growth and maintenance of tumors [30]. Through this mechanism, the overexpression of Trx1 in the BC patients makes it possible to selectively identify and quantify Trx1 as a potential biomarker for BC. By confirming the levels of Trx1, the selective identification of BC patients becomes feasible.

DxMe® BC Kit (E&S Healthcare, BCE01, Korea) is a BC diagnostic kit that utilizes the principles mentioned above. In a previous study, our research team provided clinical evidence for the efficacy of BC diagnosis using Trx1 with the aid of this device [31]. Clinical trials have demonstrated that the DxMe® BC Kit exhibits high performance, with both sensitivity and specificity exceeding 95 %. The Cut-off value for Trx1, indicative of the boundary between normal individuals and BC patients, has been determined to be 11.4 ng/mL.

However, the DxMe® BC Kit, being an enzyme-linked immunosorbent assay (ELISA) kit for semi-quantitative measurement of Trx1, is limited to intended users with specialized lab skills, typically requiring expertise from professionals [32]. Moreover, the necessity for an ELISA reader device for absorbance measurements makes it challenging to implement in small-scale clinical settings. While the time required for patients to receive diagnostic results has been significantly reduced compared to MMG, it still poses a considerable time constraint.

In light of these challenges, our research team has committed to developing a kit tailored for point-of-care test (POCT) in smaller hospitals, aiming for simplicity and rapid result confirmation, effectively addressing the outlined issues. According to recent research trends, various rapid diagnostic kits for POCT are being developed, and their potential applications are being confirmed in various fields [33–37]. Especially, in the aftermath of the recent COVID-19 pandemic, strip-type devices utilizing the lateral flow immunoassay (LFIA) method have demonstrated a paradigm shift in the next-generation diagnostic device platform, emphasizing user convenience and providing rapid and accurate results [38–42]. The detection of Trx1 using the LFIA method has been previously investigated by M. J. Lee, et al. [43]. Their research introduced an excellent automated ELISA-based LFIA kit, demonstrating a detection limit of as low as 4.1 ng/mL. However, due to the complex device fabrication process and the requirement for the simultaneous use of three different solutions, it is believed that adoption in medical settings may be challenging due to reduced user-friendliness.

This study aims to successfully differentiate BC patients from normal individuals in real clinical settings using the BC rapid diagnostic kit developed for POCT, named Elichip, derived from Enzyme-mimetic nanoparticle employed Lateral-flow Immunoassay chip. The paper details the fabrication process and characteristics of Elichip. When the concentration of Trx1 in human serum is below the cut-off value, no signal is generated, resulting in a 'negative'. Conversely, when the concentration exceeds the cut-off value, a signal is produced, leading to a 'positive'. In this study, H-Pt-Nanozyme (H-Pt-NZ) is employed as the detection label to generate the signal instead of generally used gold nanoparticles (AuNPs). H-Pt-NZ is a hierarchically structured enzyme-mimetic nanoparticle that particularly exhibits peroxidase-like activities [44]. H-Pt-NZ can amplify signals through enzymatic-substrate reactions, providing the potential to enhance sensitivity by utilizing colorimetric reactions in cases where visual discernment of diagnostic results is not feasible.

2. Materials and method

2.1. Reagents and equipment

The 400 ppm of H-Pt-NZ was obtained from NIET (11130, Daejeon, South Korea), and 40 nm diameter AuNPs were purchased from Nanocomposix (AUCR40, San Diego, USA). Bovine serum albumin (BSA) (A3803), Sodium azide (S2002), Potassium phosphate monobasic (P0662), Potassium phosphate dibasic (P3786), Sucrose (S5016), and Tween 20 (P1379) were procured from Sigma-Aldrich (Massachusetts, USA). Phosphate-buffered saline (PBS) was obtained from Welgene (LB 001–02, Gyeongsan, South Korea). Two monoclonal recombinant antibodies against Trx1, anti-Trx1 antibody 1 (Capture Ab, CAb), and anti-Trx1 antibody 2 (Detection Ab, DAb), were produced by using the ExpiFectamine™ CHO Transfection Kit (Gibco, A29129, CA, USA), and purified by ÄKTA pure™ (Cytiva, 29018224, MA, USA) and HiTrap Protein G HP column (Cytiva, 17040503, Uppsala, Sweden). Concentration of purified antibodies were confirmed by using Quickdrop (Molecular Devices, 5047178, CA, USA). Goat anti-mouse IgG antibody was acquired from ThermoFisher (A16068, Waltham, USA). Recombinant Trx1 was obtained from Ybiologics (AR-0141, Daejeon, South Korea), and artificial serum was purchased from Utak (35700-SMX-S(F), Santa Clarita, USA). Nitrocellulose membranes were procured from Sartorius (CN140, Göttingen, Germany). Other materials utilized included polyester fiber sample pads (Grade 8964, Ahlstrom, Helsinki, Finland), conjugation Pad (6613H, Ahlstrom, Helsinki, Finland), backing cards (LBN-BCR-60, LABNARA), and absorbent pads (3017–915, Whatman, Maidstone, UK). Reagent dispensing was conducted using a dispenser obtained from Biodot (ZX10100140, Irvine, USA). Images were captured using an imager purchased from Davinch-k (CG-550, Seoul, South Korea).

2.2. Recombinant antibody production in ExpiCHO cells

Recombinant antibodies CAb and DAb were produced using the CHO Transfection Kit. ExpiCHO cells were seeded at a density of 6×10^6 viable cells/mL in expression media, and heavy and light plasmid DNA were used at concentrations of 0.5 μg/mL each. Expifectamine was applied at a concentration of 3.2 μL/mL. DNA/Expifectamine complexes were dropped onto the media, and transfected ExpiCHO cells were incubated for 8 days at 37 °C, 8 % CO_2, with shaking at 125 rpm. Additional enhancer and feed were added 18 h later from the initiation of transfection. After 8 days, clear media samples were obtained following the removal of cells and debris. Subsequently, media samples were purified using ÄKTA pure™ and HiTrap Protein G HP column. CAb was dialyzed in PBS (pH 7.4) and DAb was dialyzed in 0.1 M potassium phosphate buffer (PPB, pH 7.7). Finally, antibody concentrations were determined using Quickdrop, based on absorbance at 280 nm and the extinction coefficient.

2.3. Detection label conjugation

In the present study, H-Pt-NZ was employed as a detection label, and it was utilized in conjugation with antibodies to enable result verification. H-Pt-NZ particles were synthesized with a size of 30 nm to optimize efficiency in both migrations within the porous nitrocellulose membrane and enzyme reactions. However, depending on the intended application, the particle size can be flexibly controlled by adjusting the ratio of the particle synthesis solution as described in Fig. 1 (a)-(c). Also, maintaining a consistent size is more easily achievable compared to conventional AuNPs as shown in Fig. 1 (d) and (e). Furthermore, H-Pt-NZ allows for signal amplification through enzyme reactions, potentially enabling the enhancement of the sensitivity of the device.

In this study, to facilitate comparison with traditionally utilized AuNPs as detection labels, both H-Pt-NZ and AuNPs were individually coupled with antibodies. Fundamentally, both H-Pt-NZ and AuNPs physically bind to antibodies through electrostatic forces. In a brief procedure, 10 μg of DAb was introduced into 125 μL of H-Pt-NZ. Next, 0.1 M PPB was added at a 5 % final ratio (v/v) without delay. The solution was gently mixed for 10 min. Subsequently, a PPB containing 10 % BSA was prepared, resulting in a final BSA concentration of 1 % in the solution. The mixture was gently stirred for 30 min. Following this, the conjugate mixture underwent centrifugation at 10,000 rpm for 10 min. The supernatant was then discarded, and the pellet was resuspended in 100 μL of a solution comprising 1 % BSA, 20 % sucrose, and 0.05 % sodium azide in PPB. The conjugate mixture was stored at 4 °C. The solution containing AuNPs conjugated with antibodies was also prepared using the same protocol as described above.

2.4. Fabrication of device

The device specifications are depicted in Scheme 1 (a). Following the detection label conjugation step, the prepared conjugate mixture was promptly applied to the conjugation pad and dried for a minimum of 3 h at 37 °C. Conjugation pads were stored at room temperature (RT) and under 10 % relative humidity (RH). The strip assembly was finalized by combining the prepared conjugation pad with the backing card, nitrocellulose membrane, sample pad, and absorbent pad. Using the dispenser, anti-mouse IgG antibody at a concentration of 50 μg/mL and CAb at a concentration of 100 μg/mL were dispensed onto the nitrocellulose membrane, serving as the control line (C line) and test line (T line), respectively. Finally, the prepared strips were stored at RT and under 10 % RH.

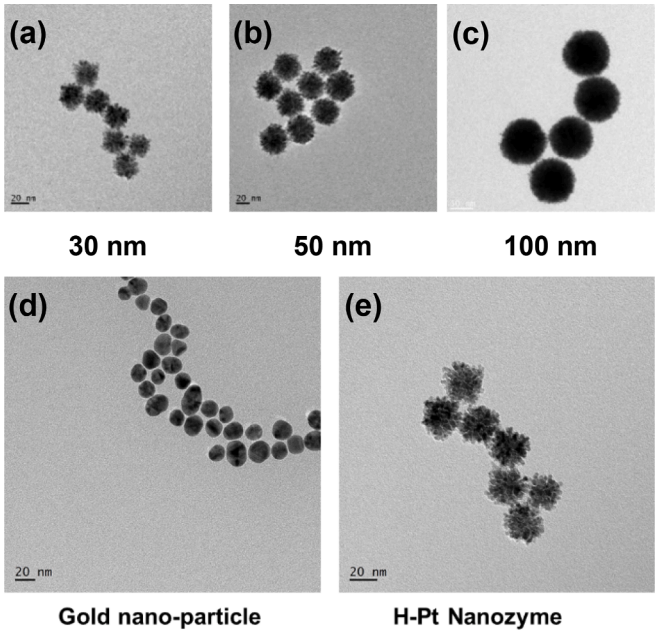


Fig. 1. Transmission electron microscopy (TEM) analysis of H-Pt-NZ and AuNPs. H-Pt-NZ can be synthesized with diameters of (a) 30 nm, (b) 50 nm, and (c) 100 nm, and by altering the composition of the particle synthesis solution, it can be synthesized in even more diverse sizes. When examining the particle size distribution, it is evident that the particle size of (d) AuNPs is less consistently synthesized compared to (e) H-Pt-NZ.

2.5. Serum sample preparation

The blood samples utilized in this study were obtained and stored at the Human Body Resources Bank of Chungnam National University Hospital. BC patient samples were collected from individuals who had received a confirmed diagnosis of BC through biopsy examination following MMG. Additionally, samples from normal individuals were collected from those confirmed during regular health check-ups to have no history of cancer or breast-related disorders through breast palpation and MMG. The protocols for participant recruitment and blood sample collection were approved (CNUH2017-12–035) by an ethical committee at Chungnam National University Hospital in Daejeon, Korea. The study with the blood samples was conducted in adherence to the relevant guidelines and regulations, with the informed consent of the patients. The separated serum was immediately aliquoted into a 1.5 mL tube and subsequently stored at −70 °C or lower for the serum stability.

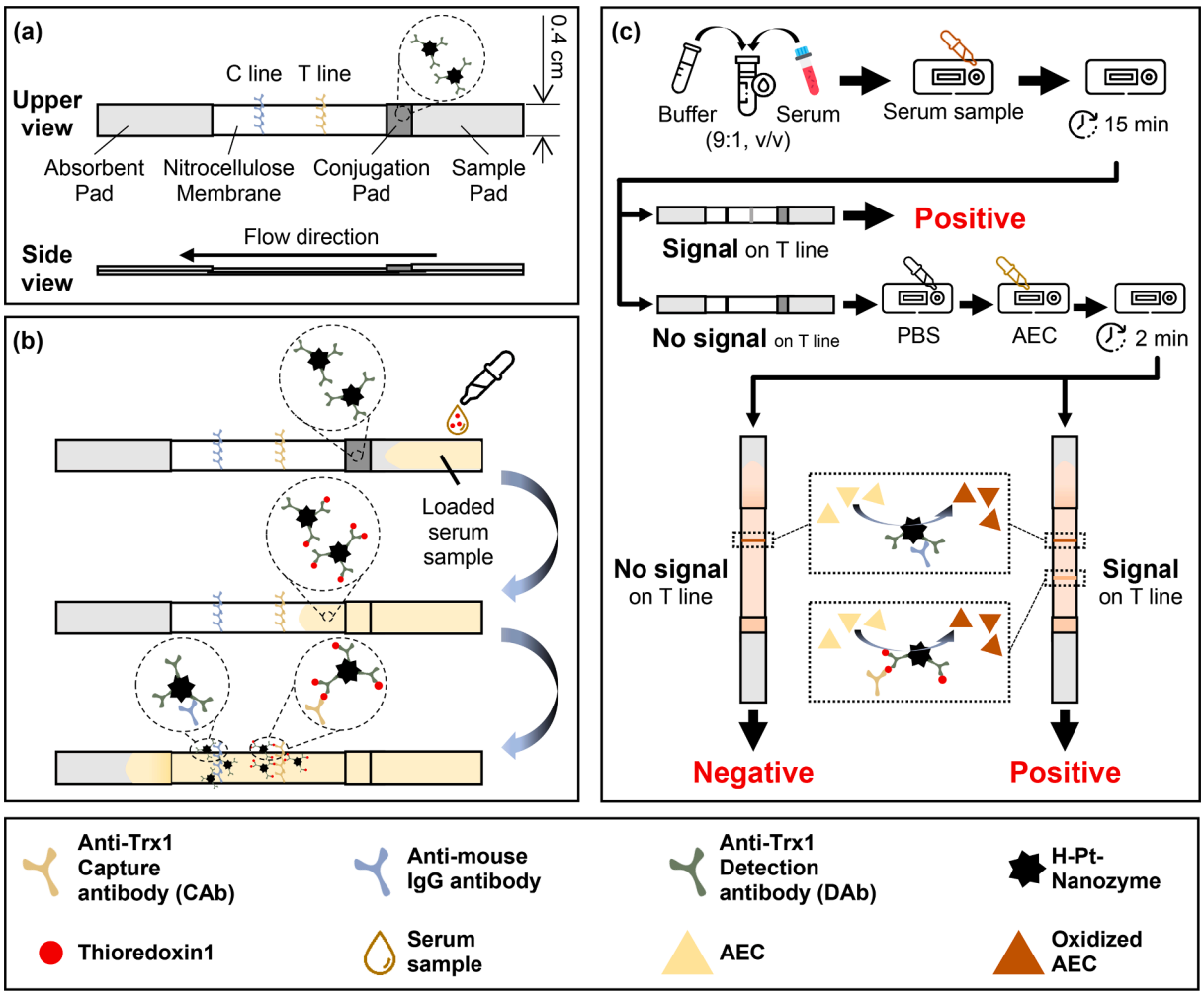
To further verify the test results of positive samples with low levels of Trx1, serum samples spiked with Trx1 were prepared. The samples used in this study consisted of single donor human serum purchased from Innovative Research (ICSERS10ML, Michigan, USA), and serum collected from two individual donors was utilized, respectively. Initially, the concentration of Trx1 was measured using the DxMe® BC Kit. Subsequently, recombinant Trx1 was spiked into the samples to achieve concentrations of 12, 20, and 25 ng/mL.

2.6. Immunoassay

The basic immunoassay principle is described in Scheme 1 (b). The fundamental principle is as follows: When a serum sample is loaded, Trx1 within the sample reacts with the H-Pt-NZ-DAb conjugate mixture on the conjugation pad, leading to the formation of H-Pt-NZ-DAb-Trx1 conjugates. This mixture then interacts with CAb immobilized on the T line, generating a signal. Additionally, the antibody immobilized on the C line consistently generates a signal as it interacts with DAb, irrespective of the Trx1 concentration in the sample.

The overall Elichip protocol and the method for interpreting the results are depicted in Scheme 1 (c). Taking into account the viscosity of human serum for the smoother fluid migration, a solution was prepared by diluting the serum to 1/10 (v/v) using 1 % Tween 20 in PBS (1 % PBST), and this diluted solution was utilized as the test sample. The results were assessed based on the visibility of a T line after 15 min from the initiation of 100 μL sample loading. A higher concentration of Trx1 in the sample results in a distinct T line, while a lower concentration leads to an invisible T line.

If the signal is not visually confirmed on the T line after 15 min of loading the sample onto the device, 3-Amino-9-Ethylcarbazole (AEC) was used to amplify the signal. The H-Pt-NZ, which acts similarly to enzymes, oxidizes multiple molecules of AEC per particle, resulting in the formation of oxidized AEC, which exhibits a strong, visible reddish-brown color. As a result, the signal intensity of the T line is amplified. The experimental procedure is outlined as follows: Initially, AEC powder was dissolved in 0.05 M acetate buffer to prepare a solution at 0.8 mg/mL, followed by mixing it with H_2O_2 at a 50:1 ratio (v/v). After incubating the Trx1 sample for 15 min, it is washed with 50 μL of PBS. Subsequently, 50 μL of AEC solution is applied between the T line and the C line. Signal confirmation at the T line was then performed after an additional 2-minute interval.



Scheme 1. The specifications of Elichip and the principles of interpreting breast cancer diagnosis results using Elichip.

2.7. Image analysis

After the sample was loaded, image capture was conducted to assess the performance of the device using Imager. In the experiment, images were captured by illuminating with a white light source for 411 msec. The captured images were processed using the gel analyzing function in Image J software to generate a plot that included the C line and T line. Lastly, the peak area of the T line was quantified from the generated plot [45–47].

3. Results

3.1. Optimizing pH at conjugation protocol of H-Pt-NZ with DAb

Antibodies undergo changes in surface charge distribution based on the solution's pH, resulting in variations in binding efficiency when conjugating with nanoparticles. Different antibodies exhibit varying optimal pH levels for binding efficiency, necessitating the need for optimization to determine the specific pH that yields optimal binding efficiency for each antibody [48,49].

In this study, optimal pH conditions were determined by observing the behavior of a solution consisting of H-Pt-NZ and antibodies mixed with sodium chloride (NaCl). NaCl has the property of reducing electrical repulsive interaction between nanoparticles, causing them to aggregate [50,51]. H-Pt-NZ, being black nanoparticles, would result in a uniformly dark-colored solution when well-bound with antibodies (Fig. 2 (a)), while inadequate binding would lead to precipitation over time, resulting in a relatively transparent solution (Fig. 2 (b)). The experimental protocol was as follows: H-Pt-NZ and antibodies, along with 0.1 M PPB at pH 6.0, 7.0, 8.0, and 9.0, were gently mixed for 10 min. Subsequently, 10 % NaCl solution was added to each solution at a 1:1 (v/v) ratio, followed by another gentle mixing for 10 min. The transmittance of each solution was then observed using a spectrophotometer, with a solution composed of PBS and 10 % NaCl in a 1:1 (v/v) ratio used as the background.

The result is shown at Fig. 2 (c) and (d). In visual inspection, appropriate conjugation was observed except at pH 6.0. Through precise transmittance measurements, it was determined that pH 9.0 exhibited the lowest transmittance in the visible spectrum, indicating optimal conjugation efficiency. However, at pH 9.0, there is a potential for antibody denaturation, leading to a decrease in affinity [52–54]. Therefore, pH 8.0, where the transmittance difference is minimal, was chosen as the optimal condition.

3.2. Detection range adjustment

Trx1 is a protein that regulates intracellular ROS levels and is a type of plasma protein that is detectable in trace amounts even in healthy individuals. Therefore, in this study, it is not about determining the presence or absence of serum Trx1, but rather qualitatively determining whether the serum Trx1 level is above or below the cut-off value of 11.4 ng/mL. Hence, deliberate adjustment of the detection range is necessary. In this study, Trx1 was spiked into artificial serum to prepare a concentration corresponding to the cut-off value of 11.4 ng/mL [31].

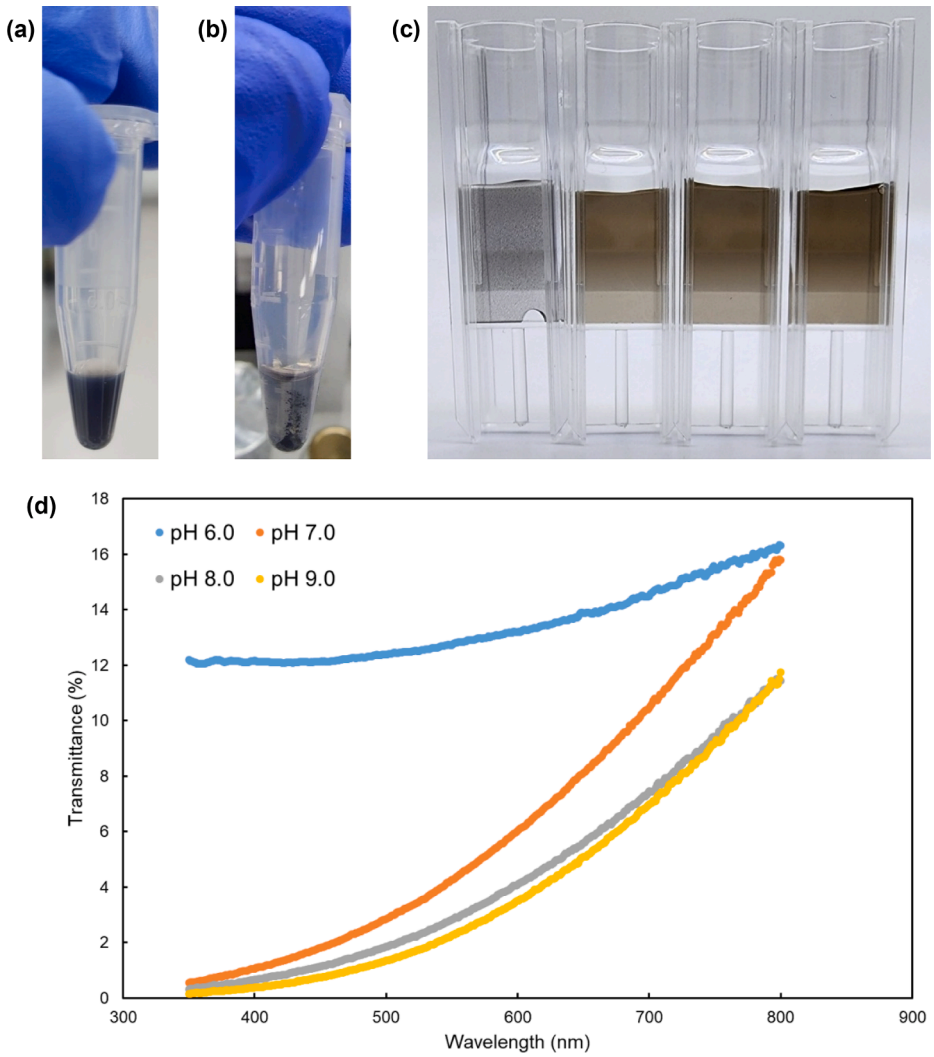


Fig. 2. Variation in appearance according to the conjugation of H-Pt-NZ and DAb. (a) When conjugation proceeds well, the solution appears in a dark color. (b) In cases where conjugation is not successful, the solution exhibits a relatively transparent color. (c) From left to right, images of solutions after conjugating H-Pt-NZ and DAb under pH conditions of 6.0, 7.0, 8.0, and 9.0, followed by the addition of NaCl to the cuvette. (d) Transmittance of solutions subjected to conjugation under each pH condition.

Using this sample, devices with different detection ranges were fabricated and compared. The detection range was adjusted by changing the concentration of CAb applied to the T line on the nitrocellulose membrane. Fig. 3 shows the results of loading the prepared sample on devices with different concentrations of CAb. The numbers at the top of the figure indicate the concentration (μg/mL) of CAb applied to the T line. Upon naked-eye observation through this experiment, the visible threshold of 11.4 ng/mL Trx1 was confirmed on the device with a CAb

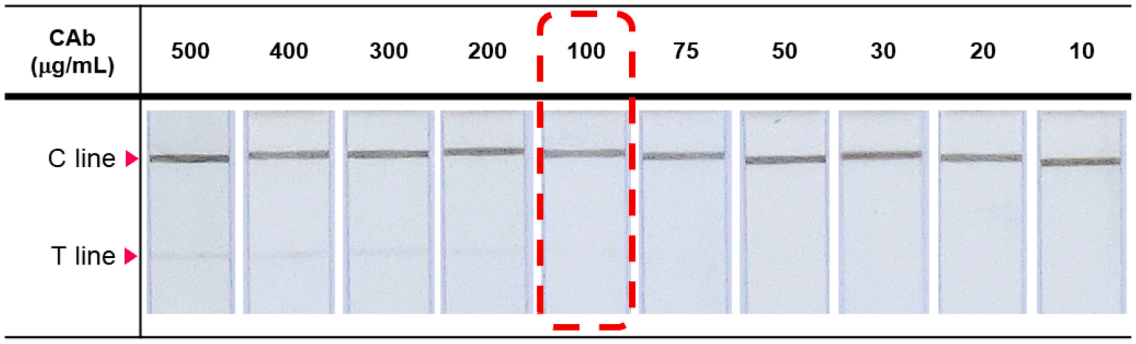


Fig. 3. Results of developing serum samples onto devices dispensed with different concentrations of CAb. The serum samples were prepared with Trx1 spiked artificial serum, adjusted to a concentration of 11.4 ng/mL, and diluted 1/10 (v/v) with a 1 % PBST solution. Upon naked-eye observation through this experiment, the visible threshold of 11.4 ng/mL Trx1 was confirmed on the device with a CAb concentration of 100 mg/mL (red dashed line). (For interpretation of the references to color in this figure legend, the reader is referred to the web version of this article.)

concentration of 100 μg/mL. Therefore, the concentration of CAb in the device was determined to be 100 μg/mL.

3.3. Comparative analysis of performance between devices utilizing AuNPs and H-Pt NZ

Given the relatively unfamiliar status of H-Pt-NZ as a detection label, it is imperative to explore its immunoassay performance, particularly in contrast to the conventionally established AuNPs. To verify the immunoassay performance, the limit of detection (LOD) was evaluated. In this study, in order to make a comparison under the same conditions, the signal amplification process using AEC was not conducted in this experiment. Trx1 was diluted into concentrations of 5, 10, 20, 40, 80, 160, and 320 ng/mL using artificial serum. The immunoassay was conducted in quintuplicate at each Trx1 concentration. The LOD was determined by adding three times the standard deviation (SD) to the mean background [55,56]. Fig. 4 represents the calibration curves generated by loading Trx1 spiked artificial serum samples on devices that use (a) H-Pt-NZ and (b) AuNPs, respectively. Both devices achieved LOD below the cut-off value of 11.4 ng/mL. Due to the use of imager for detection, concentrations that are not visible to the naked eye were also accurately quantified. This confirms that both devices can qualitatively distinguish between BC and normal cases. Therefore, it can be noted that the device using H-Pt-NZ exhibits performance similar to the device using AuNPs.

3.4. Signal amplification by enzyme reaction

The extent to which the serum Trx1 concentration increases in BC patients varies among individuals. Consequently, there may be cases where individuals are diagnosed as BC patients, yet their Trx1 concentration closely approximates the cut-off value of 11.4 ng/mL. Moreover, in some instances, Trx1 levels may remain below 11.4 ng/mL, leading to a higher likelihood of false-negative results, even when measured under normal processes. To mitigate such cases, it is imperative to enhance the sensitivity of the diagnostic device. As suggested in the text, one means of achieving increased sensitivity is through the utilization of enzyme reactions to amplify the signal intensity.

Prepared AEC solution was utilized to amplify the generated signal by Trx1 sample on the device. For the Trx1 sample, artificial serum was used to dilute concentrations to 6 and 12 ng/mL, serving as negative control (NC) and positive control (PC), respectively. The results, as shown in Fig. 5, demonstrate that before the application of AEC solution, the device developed with PC did not exhibit a T line signal; however, after AEC application, a discernible T line signal was observed. In contrast, both before and after AEC application, the device developed with NC did not show any T line signal.

3.5. Clinical serum sample comparison

The serum samples stored at −70 °C were gradually thawed stepwise at −20 °C, 4 °C, and RT, with a minimum of 1 h at each temperature. Clinical information for each serum sample donor can be found in Table 1. Fig. 6 illustrates the results obtained from the loading of (a) BC samples and (b) normal samples on the device. The figures are labeled with letters (starting with A) at the top, indicating the donor numbers of each sample. It was observed that the device with BC samples showed a signal at the T line, while the device with normal samples did not exhibit a signal. Therefore, only the device where the signal was not visible on the T line for the normal sample was further treated with AEC to confirm. After 2 min of AEC treatment, the photo was taken (Fig. 6 (c)). As a result, no signal was observed on the normal sample loaded device, confirming the absence of false positives.

Next, single donor human serum samples were prepared by mixing recombinant Trx1 to adjust the concentration. Serum samples from two donors were measured for Trx1 concentration using the DxMe® BC Kit,

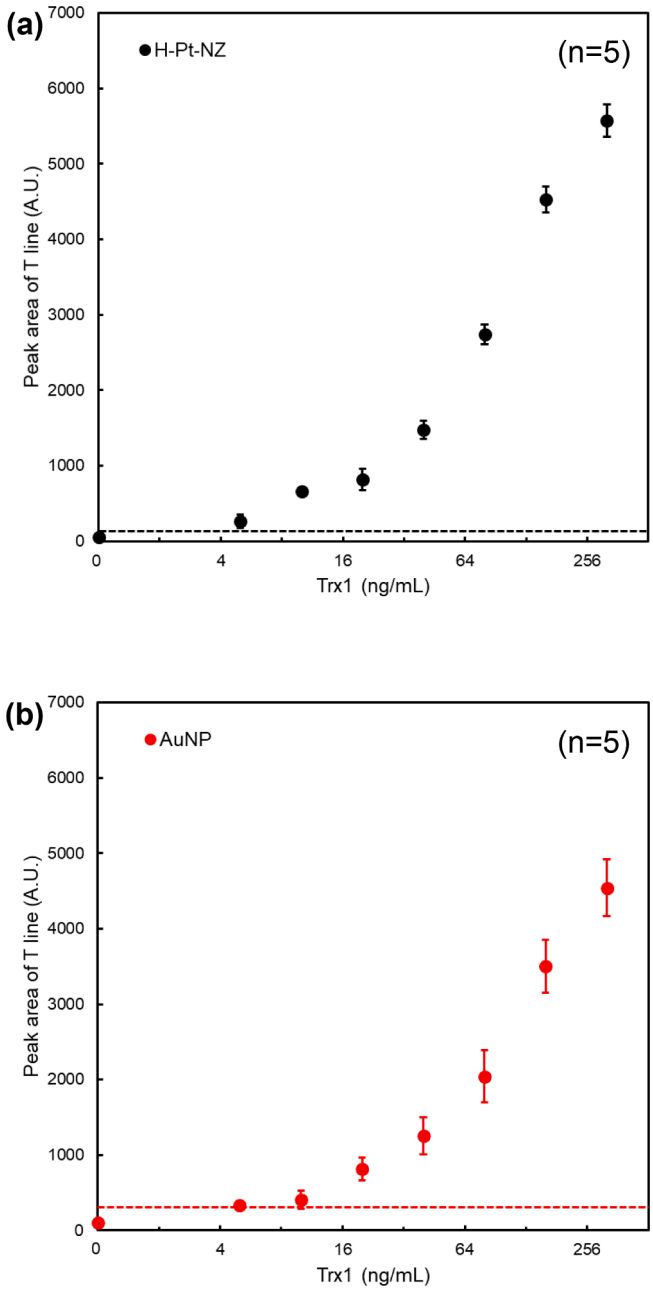


Fig. 4. Calibration curves generated by loading Trx1 spiked artificial serum samples on devices that use (a) H-Pt-NZ and (b) AuNPs, respectively. The dashed line represents the LOD, defined as the value obtained by adding three times of the SD to the mean of the background.

resulting in 7.18 ng/mL and 4.25 ng/mL, respectively. Using each serum, samples with Trx1 concentrations of 12, 20, and 25 ng/mL were prepared. After developing each sample, the T line signal was clearly visible in strips developed with Trx1 concentrations of 20 and 25 ng/mL. However, for the 12 ng/mL concentration, the signal was barely visible (Fig. 7 (a)). Subsequently, upon confirming after application of the AEC solution, a clear signal was observed even at the 12 ng/mL concentration (Fig. 7 (b)).

4. Discussion

BC is a type of cancer with a 99 % 5-year relative survival rate when diagnosed early through screening [4,57], making early and accurate diagnosis essential. In light of this, the Elichip developed in this study

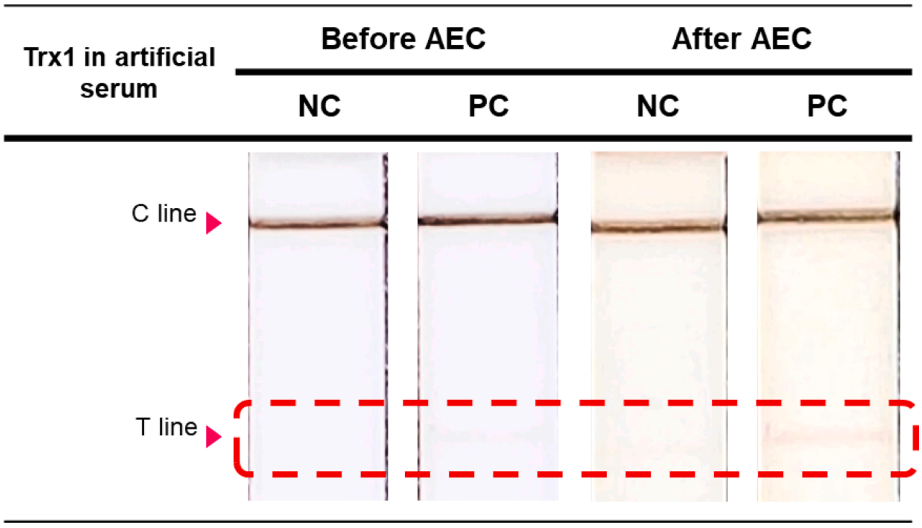


Fig. 5. Comparison of the Elichip after developing artificial serum samples before and after the application of AEC. NC and PC contain 6 and 12 ng/mL of Trx1, respectively. The "Before AEC" image was captured 15 min after deploying the artificial serum sample on the prepared Elichip. Subsequently, AEC solution was applied to the midpoint between the T line and C line, and the "After AEC" image was taken 2 min later. The results were confirmed based on the color development at the T line (red dashed line). (For interpretation of the references to color in this figure legend, the reader is referred to the web version of this article.)

Table 1
Detailed clinical information including Trx1 concentration for each donor. The concentration of Trx1 was measured using the DxMe® BC Kit. BI-RADS indicates the potential malignancy risk of tumors based on the diagnostic results of MMG and US. TNM staging involves the size of the Tumor, lymph Node involvement, and Metastasis to other organs. Stages are determined based on TNM staging. Upon confirming the stages and corresponding TNM staging for 10 cancer patients, Elichip successfully distinguished patients in the early stages of cancer.

Type	Sample No.	Age	Sex	Hormone-receptor			BI-RADS	STAGE	TNM stage			Trx1 concentration(ng/mL)
				ER	PR	HER2			T	N	M	
BC	A0401	74	female	p	p	p	5	2A	T2	N0	M0	31.27
	A1061	60	female	n	n	p	2	2A	T2	N0	M0	39.36
	A2098	45	female	p	p	p	1	1A	T1	N0	M0	40.35
	A1825	44	female	p	p	n	4	1A	T1	N0	M0	39.22
	A0903	76	female	p	p	n	4	1A	T1	N0	M0	31.36
	A1007	63	female	p	p	p	5	3A	T3	N2	M0	43.98
	A0274	55	female	p	p	p	4	2B	T2	N1	M0	48.98
	A2728	70	female	p	p	n	4	1A	T1	N0	M0	42.07
	A2065	72	female	p	p	p	4	1A	T1	N0	M0	34.40
	A0283	52	female	n	n	p	4	0	Tis	N0	M0	38.52
Normal	A2958	57	female				1					2.45
	A2676	41	female				1					2.42
	A2123	49	female				1					2.34
	A1266	68	female				1					1.78
	A0013	50	female				1					2.59
	A1879	61	female				1					2.31
	A2705	65	female				1					1.86
	A0076	55	female				2					1.95
	A2518	50	female				1					1.50
	A2069	65	female				2					1.59

demonstrates notable advantages, allowing for rapid diagnosis using a small sample size. In addition, despite the limited number of samples, it effectively distinguished between BC patients and healthy individuals, suggesting its potential as a BC screening tool.

However, Trx1, being a relatively recently discovered biomarker, requires further scientific discussion before immediate application in clinical settings. First of all, it is crucial for us to clarify the future role of Elichip as an in-vitro diagnostic medical device and determine its intended purpose.

According to the definitions provided by the Global Harmonization Task Force (GHTF), an in-vitro diagnostic medical device needs to establish one of the following eight intended purposes: Diagnosis, Aid to Diagnosis, Screening, Monitoring, Predisposition, Prognosis, Prediction, and Determination of Physiological Status [58]. Given the rapid and user-friendly diagnostic capabilities of Elichip, both Screening and Aid to Diagnosis are suitable. The most significant difference between Screening and Aid to Diagnosis lies in the intended target users of the medical device, whether it is designed for asymptomatic individuals (Screening) or symptomatic individuals (Aid to Diagnosis). Hence, there arises a necessity to scrutinize the diagnostic methodology for both objectives in the present phase and evaluate the potential utility of Elichip.

The diagnostic procedures based on the presence or absence of symptoms can be found in the National Comprehensive Cancer Network (NCCN) guideline for BC screening and diagnosis [59]. First of all, the schematic summary of diagnostic guidelines for asymptomatic women proposed by NCCN, as shown in Scheme 2 (a), guides different diagnostic procedures based on the Breast Imaging-Reporting and Data System (BI-RADS) category typically evaluated from Screening MMG results. In cases of dense breast tissue, it can be challenging to detect

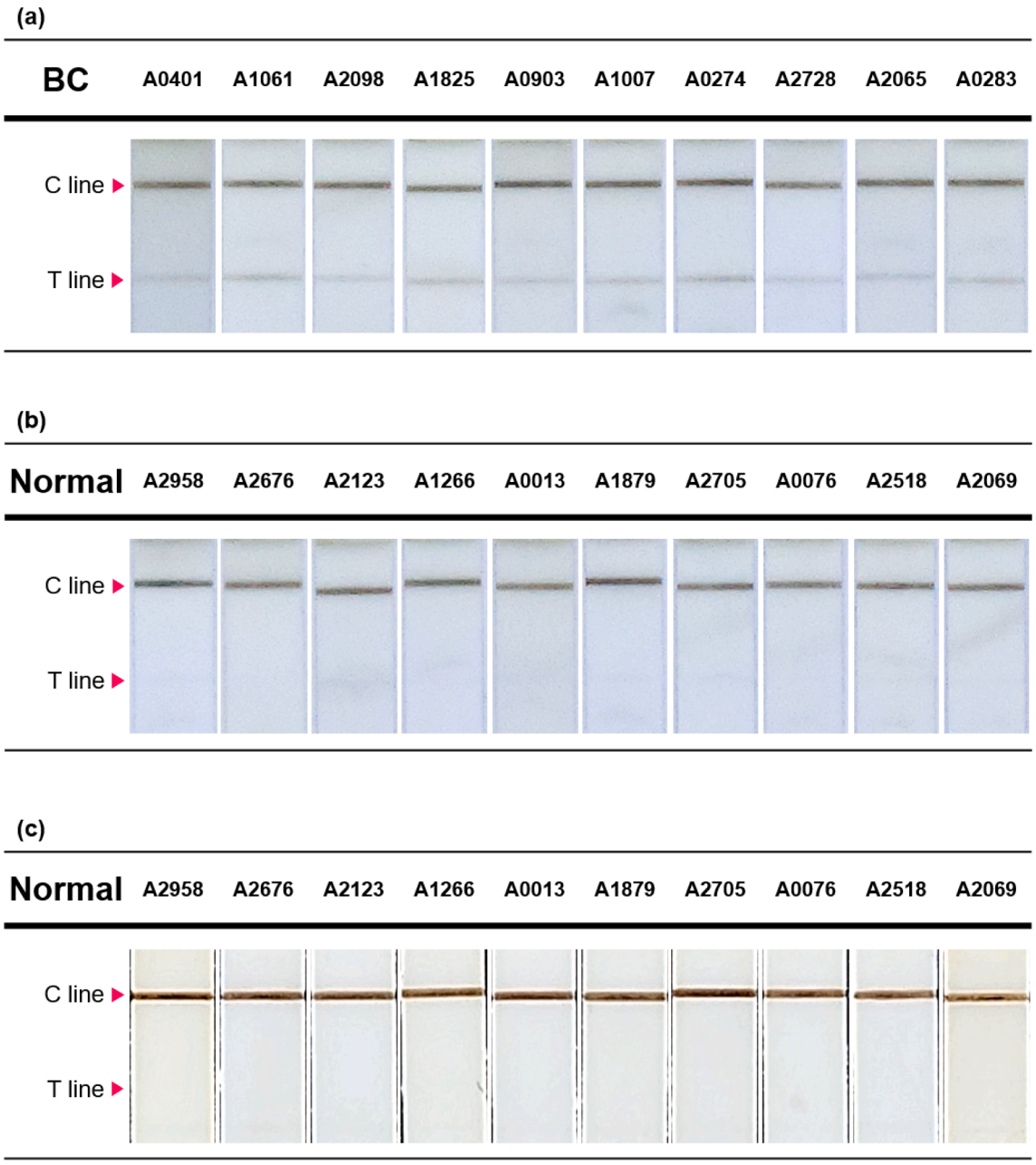


Fig. 6. The results obtained from the loading of (a) BC samples and (b) Normal samples on the Elichip. After developing the serum sample for 15 min, it was visually confirmed that there was no signal on the T line of Elichip for normal serum. Therefore, (c) AEC solution was applied only to the Elichip with normal serum, and the results were checked after 2 min. The letters starting with 'A' above strips represent the donor numbers of each sample.

malignant tumors, leading to a false-negative (BI-RADS 1, 2). If subsequent Screening MMG is scheduled 1–2 years later after receiving a negative diagnosis, there is a risk that the lesion may have progressed. In this study, samples from patients confirmed as Elichip positive, specifically A2098 and A1061, had received BI-RADS 1 and 2 classifications (Table 1). This confirms that Elichip has the potential to improve the false-negative rate. Furthermore, in the case of BI-RADS 3, additional diagnostic mammography (DMMG) and ultrasonography (US) are recommended. As a result of these additional examinations, approximately 2 % of women receive a diagnosis of malignant tumors [60]. Unfortunately, in this study, there were no BC specimens corresponding to BI-RADS 3, making it impossible to confirm the false-negative status.

If Elichip is used in the screening phase, it can assist in enhancing the sensitivity by complementing the high false-negative rate of screening MMG. Additionally, when clinical suspicion is involved, particularly in cases of BI-RADS 3 where there is a potential for malignant tumors, the results from Elichip can be considered (Scheme 2 (b)).

Next, the diagnostic procedure for symptomatic women is summarized as depicted in Scheme 3 (a), where the subsequent diagnostic steps are determined through DMMG and US. In cases where DMMG and US yield negative results, the decision for core needle biopsy or further observation is made based on the clinical suspicion. If either DMMG or US shows a positive result, a core needle biopsy is recommended.

In cases where clinical suspicion is required, the utilization of Elichip can aid in distinguishing false negatives, guiding appropriate follow-up diagnostic procedures. Moreover, in cases where there is a difference between the results of DMMG and US, employing Elichip can complement the high false positive rate of US results, potentially reducing false positives before core needle biopsy and preventing unnecessary surgeries (Scheme 3 (b)). Furthermore, the specimens from BC patients in

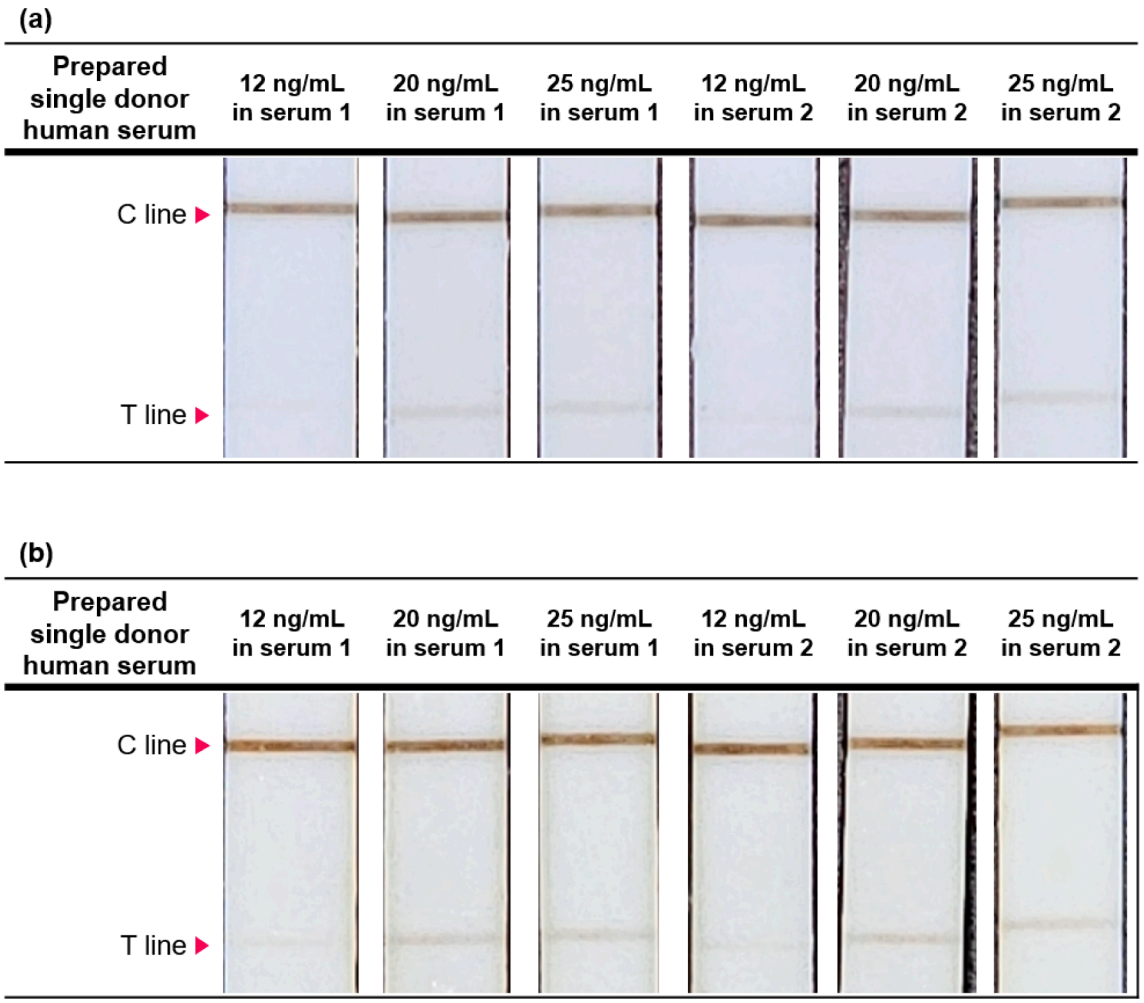


Fig. 7. (a) Results of loading each single donor human serum prepared by adjusting the Trx1 concentration onto Elichip. (b) Results after applying AEC on the developed Elichip.

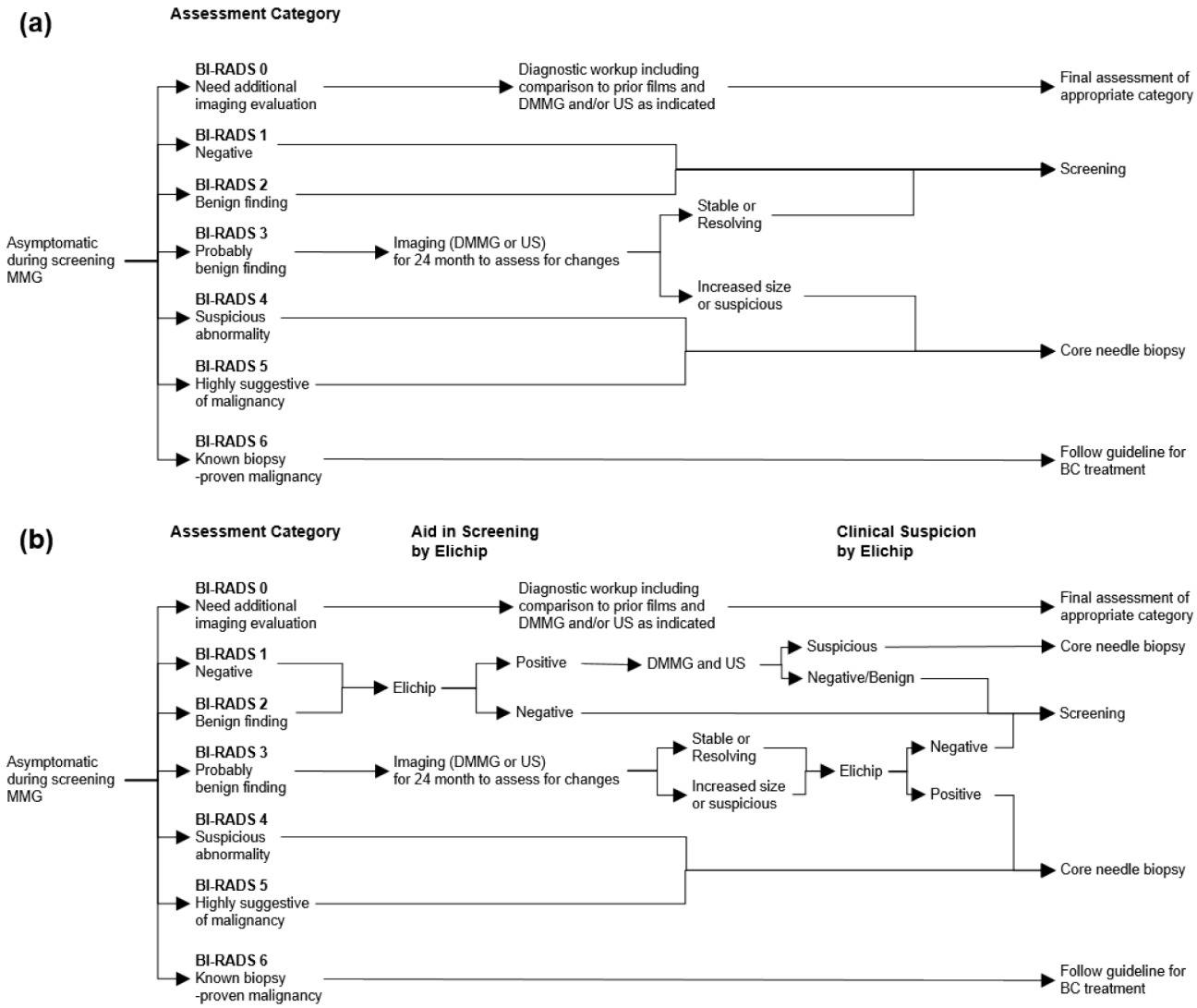
stages 0 and 1 used in this study were also determined as Elichip positive (Table 1), indicating the potential advantages of Elichip in early BC diagnosis.

To achieve the above stated objectives, Elichip needed to exhibit excellent sensitivity and specificity. In this study, to potentially enhance sensitivity in future applications, H-Pt-NZ was chosen over the commonly used AuNPs. When comparing the device utilizing H-Pt-NZ with the one employing AuNPs, both devices exhibited nearly equivalent performance in terms of LOD (Fig. 4). However, the overall SD was lower for the H-Pt-NZ device. This is attributed to the characteristic of H-Pt-NZ, which allows for consistent production with minimal variation in particle sizes, in contrast to the larger particle size variability observed in AuNPs (Fig. 1 (d), (e)). With these characteristics, improved reproducibility is expected, enabling high precision diagnostics in real clinical settings.

Additionally, an investigation was conducted to determine the feasibility of complementing false-negative outcomes through the utilization of H-Pt-NZ and AEC for signal amplification. Upon reviewing Fig. 5, the signal from the developed strip for the PC might appear very faint, but this is attributed to the low resolution of the Imager; when observed with the naked eye, T line on the strip exhibited a distinct reddish-brown color different from the background, making it relatively easy to distinguish. Furthermore, although the color of the strip changed overall due to the diffusion of AEC, it did not pose a significant issue in distinguishing the T line. However, since the absolute intensity of the signal at the T line is still relatively weak, further research may be needed to establish the mechanism where the signal sharply intensifies at the cut-off line. Moreover, assessing the clinical efficacy of Elichip necessitates conducting additional research with a more extensive set of clinical specimens. By capitalizing on these attributes, which are not achievable in devices utilizing AuNPs, Elichip utilizing H-Pt-NZ is anticipated to reduce false-negative outcomes in real clinical settings in the future.

Moreover, interference test was conducted to further scrutinize the performance of Elichip. Interference reactions were tested for six substances. Strong interference reactions were observed with hemoglobin and whole blood, likely originating from hemoglobin. Even at lower concentrations, mild interference reactions persisted during repeated experiments with these substances. Therefore, caution is necessary to prevent hemolysis reactions when using serum samples with this kit.

Next, accelerated aging of Elichip finished product was conducted for storage stability tests. The storage stability test, according to the standard guide for accelerated aging of medical devices [61], it was confirmed that conducting accelerated aging for 15 days at 55 °C would result in a level of aging effect similar to that of storing at room temperature for 120 days. In this experiment, shaded and moisture-proofed finished products were stored in a 55 °C incubator, and accelerated aging was conducted for 17 days from the date of manufacture. Subsequently, on day 0, 7, and day 17 from the date of manufacture, a comparison of positive and negative samples was conducted using Elichip. As a result, there were no observed changes in the performance of distinguishing positive and negative samples. Therefore, it can be



Scheme 2. (a) Schematic summary of the diagnostic guidelines for BC in asymptomatic women proposed by NCCN. Asymptomatic women undergo different diagnostic procedures based on the results of screening MMG. High false-negative rates in dense breast tissue lead to additional procedures for BI-RADS 1 or 2 Moreover, BI-RADS 3 cases may necessitate clinical suspicion during additional diagnostic procedures. (b) Schematic summary of newly proposed breast cancer diagnostic guidelines for asymptomatic women utilizing Elichip. Elichip can reduce the false-negative rate for individuals classified as BI-RADS 1 or 2. Additionally, physicians can refer to Elichip results during additional diagnostic procedures for BI-RADS 3.

concluded that Elichip ensures a minimum shelf life of 4 months. The above information is detailed in the Supplementary File.

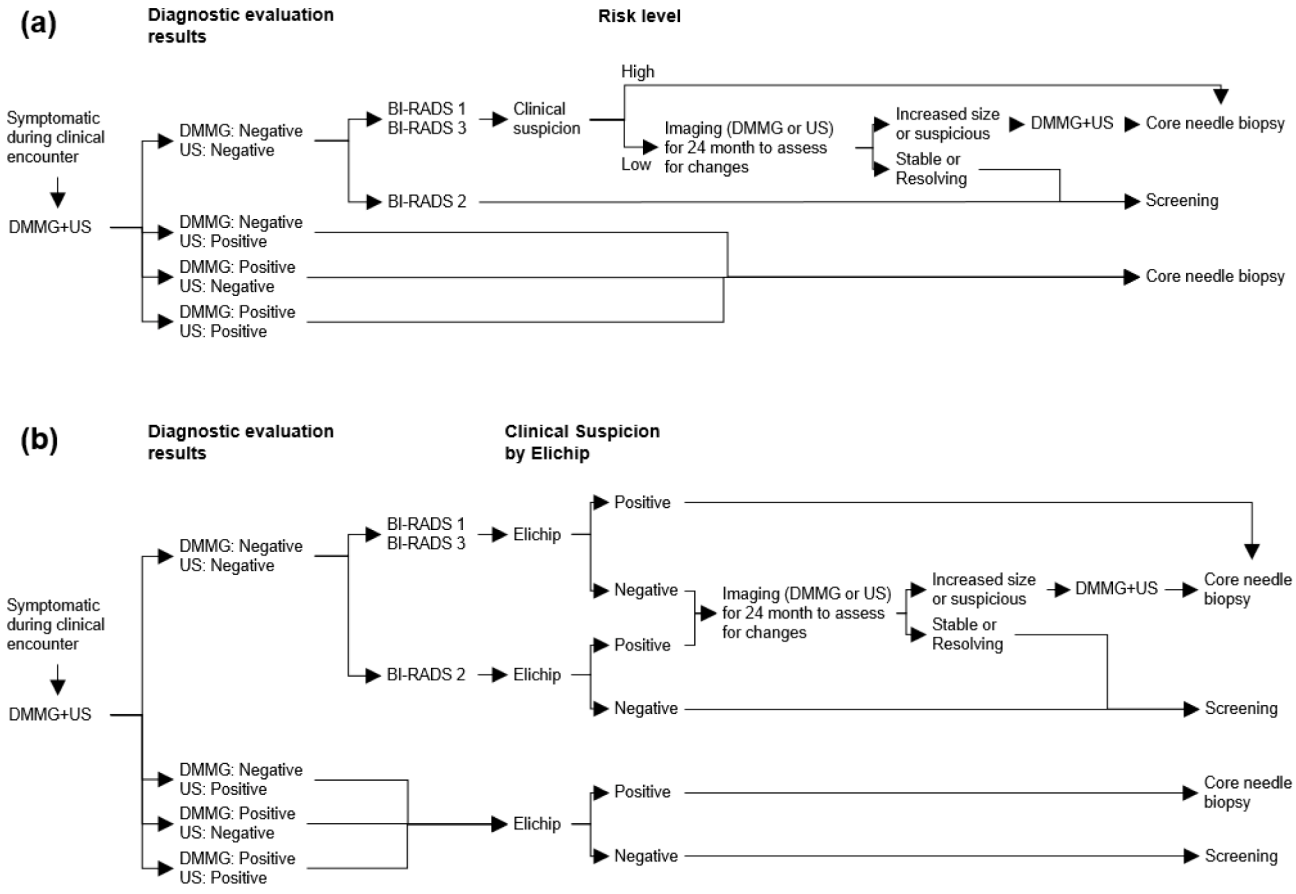
Finally, for a more detailed analysis, Trx1 concentrations in collected BC and normal samples were measured using the DxMe® BC Kit (Table 1). Upon confirmation of this, it was verified that the serum Trx1 concentrations for healthy individuals and breast cancer patients were respectively below and above cut-off value, confirming the accuracy of the test. The actual clinical samples used exhibited higher viscosity, resulting in a relatively messy background on the device (Fig. 6) compared to artificial serum (Fig. 3).

5. Conclusion

This paper describes the development of a rapid diagnostic kit for BC capable of qualitatively assessing the concentration of Trx1 in human serum. To enhance the sensitivity of the device in future applications, H-Pt-NZ was employed, and its performance was found to be superior to that of devices utilizing conventional AuNPs, as evidenced by a comparison of the LOD. Subsequent optimization of Trx1 detection involved adjusting the detection range, successfully achieving a complete separation of clinical samples, consisting of 10 each from normal individuals and BC patients. We anticipate that the Elichip developed in this study will play a crucial role in aiding clinical judgment and facilitating early diagnosis of BC. Our research team plans to conduct additional clinical trials and optimize enzyme reactions to enhance sensitivity, evaluating the feasibility of more accurate diagnosis of BC patients based on their clinical history using Elichip. In the future, we anticipate achieving more accurate diagnoses in clinical settings by improving the false-negative rate of Elichip.

CRediT authorship contribution statement

J.C. Shin: Writing – review & editing, Writing – original draft, Visualization, Methodology, Investigation, Formal analysis, Data curation, Conceptualization. **D.W. Kim:** Writing – original draft, Validation, Software, Methodology, Investigation, Formal analysis, Data curation. **S.H. Kim:** Writing – review & editing, Visualization, Supervision, Project administration, Methodology, Data curation, Conceptualization. **X. Yang:** Writing – review & editing, Visualization, Investigation, Formal analysis. **Y.G. Kim:** Writing – review & editing, Visualization,



Scheme 3. (a) Schematic summary of the diagnostic guidelines for BC in symptomatic women proposed by NCCN. Symptomatic women undergo different diagnostic procedures based on the results of DMMG and US. Even in cases where both tests are negative, clinical suspicion may lead to the core needle biopsy. (b) Schematic summary of newly proposed breast cancer diagnostic guidelines for symptomatic women utilizing Elichip. Following the diagnostic results of DMMG and US, incorporating Elichip can complement high false-positive rates associated with US, thereby preventing unnecessary surgeries.

Resources, Conceptualization. **E.A. Kang:** Writing – review & editing, Visualization, Supervision, Resources, Conceptualization. **J.A. Song:** Writing – review & editing, Supervision, Resources, Project administration, Methodology, Funding acquisition. **K.H. Suh:** Writing – review & editing, Supervision, Resources, Project administration, Methodology, Funding acquisition.

Declaration of competing interest

The authors declare that they have no known competing financial interests or personal relationships that could have appeared to influence the work reported in this paper.

Data availability

Data will be made available on request.

Acknowledgments

We sincerely express our gratitude to NIET for their support in providing the equipment and materials for this research. Additionally, we gratefully acknowledge provision of serum samples from the Human Body Resources Bank of Chungnam National University Hospital. Lastly, this study received support from the Establishment of the Collaboration Platform for the Technology-Commercialization grant funded by the Ministry of Science and ICT (MSIT, Korea) (Grant No. 2021-DD-RD-0012).

Appendix A. Supplementary data

Supplementary data to this article can be found online at https://doi.org/10.1016/j.microc.2024.110919.

References

[1] M. Arnold, E. Morgan, H. Rumgay, A. Mafra, D. Singh, M. Laversanne, J. Vignat, J. R. Gralow, F. Cardoso, S. Siesling, I. Soerjomataram, Current and future burden of breast cancer: Global statistics for 2020 and 2040, The Breast 66 (2022) 15–23, https://doi.org/10.1016/j.breast.2022.08.010.
[2] Y. Xu, M. Gong, Y. Wang, Y. Yang, S. Liu, Q. Zeng, Global trends and forecasts of breast cancer incidence and deaths, Sci. Data 10 (2023) 334, https://doi.org/10.1038/s41597-023-02253-5.
[3] H. Sung, J. Ferlay, R.L. Siegel, M. Laversanne, I. Soerjomataram, A. Jemal, F. Bray, Global Cancer Statistics, GLOBOCAN Estimates of Incidence and Mortality Worldwide for 36 Cancers in 185 Countries, CA. Cancer J. Clin. 71 (2021) (2020) 209–249, https://doi.org/10.3322/caac.21660.
[4] A.N. Giaquinto, H. Sung, K.D. Miller, J.L. Kramer, L.A. Newman, A. Minihan, A. Jemal, R.L. Siegel, Breast Cancer Statistics, 2022, CA, Cancer J. Clin. 72 (2022) 524–541, https://doi.org/10.3322/caac.21754.
[5] G. Gorini, M. Zappa, G. Miccinesi, E. Paci, A.S. Costantini, Breast cancer mortality trends in two areas of the province of Florence, Italy, where screening programmes started in the 1970s and 1990s, Br. J. Cancer 90 (2004) 1780–1783, https://doi.org/10.1038/sj.bjc.6601744.
[6] R.E. Hendrick, M.A. Helvie, D.L. Monticciolo, Breast cancer mortality rates have stopped declining in U.S. women younger than 40 years, Radiology 299 (2021) 143–149, https://doi.org/10.1148/radiol.2021203476.
[7] J.M.G. Wilson, G. Jungner, PRINCIPLES AND PRACTICE OF SCREENING FOR DISEASE, (n.d.).
[8] G. Van Schoor, S.M. Moss, J.D.M. Otten, R. Donders, E. Paap, G.J. Den Heeten, R. Holland, M.J.M. Broeders, A.L.M. Verbeek, Increasingly strong reduction in breast cancer mortality due to screening, Br. J. Cancer 104 (2011) 910–914, https://doi.org/10.1038/bjc.2011.44.

[9] World Health Organization, WHO position paper on mammography screening, World Health Organization, Geneva, 2014 https://iris.who.int/handle/10665/137339 (accessed January 10, 2024.
[10] K. Kaulback, Ontario Health Technology Assessment Series 2007; Vol, 7 (n.d.).
[11] B.K. Rimer, L.G. Bluman, The Psychosocial Consequences of Mammography, JNCI Monogr. 1997 (1997) 131–138, https://doi.org/10.1093/jncimono/1997.22.131.
[12] V.A. Loving, S. Aminololama-Shakeri, J.W.T. Leung, Anxiety and Its Association With Screening Mammography, J. Breast Imaging 3 (2021) 266–272, https://doi.org/10.1093/jbi/wbab024.
[13] B. Hafslund, Mammography and the experience of pain and anxiety, Radiography 6 (2000) 269–272, https://doi.org/10.1053/radi.2000.0281.
[14] C.I. Montoro, M.D.C. Alcaraz, C.M. Galvez-Sánchez, Experience of Pain and Unpleasantness during Mammography Screening: A Cross-Sectional Study on the Roles of Emotional, Cognitive, and Personality Factors, Behav. Sci. 13 (2023) 377, https://doi.org/10.3390/bs13050377.
[15] E. Devolli-Disha, S. Manxhuka-Kërliu, H. Ymeri, A. Kutllovci, Comparative accuracy of mammography and ultrasound in women with breast symptoms according to age and breast density, Bosn. J. Basic Med. Sci. 9 (2009) 131–136, https://doi.org/10.17305/bjbms.2009.2832.
[16] M. Løberg, M.L. Lousdal, M. Bretthauer, M. Kalager, Benefits and harms of mammography screening, Breast Cancer Res. 17 (2015) 63, https://doi.org/10.1186/s13058-015-0525-z.
[17] H.G. Welch, H.J. Passow, Quantifying the benefits and harms of screening mammography, JAMA Intern. Med. 174 (2014) 448, https://doi.org/10.1001/jamainternmed.2013.13635.
[18] C.D. Lehman, E. White, S. Peacock, M.J. Drucker, N. Urban, Effect of age and breast density on screening mammograms with false-positive findings, Am. J. Roentgenol. 173 (1999) 1651–1655, https://doi.org/10.2214/ajr.173.6.10584815.
[19] Y. Ishibashi, H. Ohtsu, M. Ikemura, Y. Kikuchi, T. Niwa, K. Nishioka, Y. Uchida, H. Miura, S. Aikou, T. Gunji, N. Matsuhashi, Y. Ohmoto, T. Sasaki, Y. Seto, T. Ogawa, K. Tada, S. Nomura, Serum TFF1 and TFF3 but not TFF2 are higher in women with breast cancer than in women without breast cancer, Sci. Rep. 7 (2017) 4846, https://doi.org/10.1038/s41598-017-05129-y.
[20] P. Li, Q. He, C. Luo, L. Qian, Diagnostic and prognostic potential of serum angiopoietin-2 expression in human breast cancer, (n.d.).
[21] B.-J. Park, M.-K. Cha, I.-H. Kim, Thioredoxin 1 as a serum marker for breast cancer and its use in combination with CEA or CA15-3 for improving the sensitivity of breast cancer diagnoses, BMC Res. Notes 7 (2014) 7, https://doi.org/10.1186/1756-0500-7-7.
[22] B.-J. Park, M.-K. Cha, I.-H. Kim, Thioredoxin 1 as a serum marker for ovarian cancer and its use in combination with CA125 for improving the sensitivity of ovarian cancer diagnoses, Biomarkers 19 (2014) 604–610, https://doi.org/10.3109/1354750X.2014.956793.
[23] M. Bhatia, K.L. McGrath, G. Di Trapani, P. Charoentong, F. Shah, M.M. King, F. M. Clarke, K.F. Tonissen, The thioredoxin system in breast cancer cell invasion and migration, Redox Biol. 8 (2016) 68–78, https://doi.org/10.1016/j.redox.2015.12.004.
[24] C. Cadenas, D. Franckenstein, M. Schmidt, M. Gehrmann, M. Hermes, B. Geppert, W. Schormann, L.J. Maccoux, M. Schug, A. Schumann, C. Wilhelm, E. Freis, K. Ickstadt, J. Rahnenführer, J.I. Baumbach, A. Sickmann, J.G. Hengstler, Role of thioredoxin reductase 1 and thioredoxin interacting protein in prognosis of breast cancer, (2010).
[25] G.B. Kallis, A. Holmgren, Differential reactivity of the functional sulfhydryl groups of cysteine-32 and cysteine-35 present in the reduced form of thioredoxin from Escherichia coli, J. Biol. Chem. 255 (1980) 10261–10265, https://doi.org/10.1016/S0021-9258(19)70458-X.
[26] C. World, O.N. Spindel, B.C. Berk, Thioredoxin-interacting protein mediates TRX1 translocation to the plasma membrane in response to tumor necrosis factor-α: A key mechanism for vascular endothelial growth factor receptor-2 transactivation by reactive oxygen species, Arterioscler. Thromb. Vasc. Biol. 31 (2011) 1890–1897, https://doi.org/10.1161/ATVBAHA.111.226340.
[27] K.C. Chu, W.F. Anderson, Rates for Breast cancer characteristics by estrogen and progesterone receptor status in the major racial/ethnic groups, Breast Cancer Res. Treat. 74 (2002) 199–211, https://doi.org/10.1023/A:1016361932220.
[28] L.K. Dunnwald, M.A. Rossing, C.I. Li, Hormone receptor status, tumor characteristics, and prognosis: a prospective cohort of breast cancer patients, Breast Cancer Res. 9 (2007) R6, https://doi.org/10.1186/bcr1639.
[29] M.-K. Cha, K.-H. Suh, I.-H. Kim, Overexpression of peroxiredoxin I and thioredoxin1 in human breast carcinoma, J. Exp. Clin. Cancer Res. 28 (2009) 93, https://doi.org/10.1186/1756-9966-28-93.
[30] L.C. Flores, M.G. Roman, G.M. Cunningham, C. Cheng, S. Dube, C. Allen, H. Van Remmen, G.B. Hubbard, T.L. Saunders, Y. Ikeno, Continuous overexpression of thioredoxin 1 enhances cancer development and does not extend maximum lifespan in male C57BL/6 mice, Pathobiol. Aging Age-Relat. Dis. 8 (2018) 1533754, https://doi.org/10.1080/20010001.2018.1533754.
[31] Y.J. Lee, Y. Kim, B.B. Choi, J.R. Kim, H.M. Ko, K.H. Suh, J.S. Lee, The blood level of thioredoxin 1 as a supporting biomarker in the detection of breast cancer, BMC Cancer 22 (2022) 12, https://doi.org/10.1186/s12885-021-09055-1.
[32] S. Hosseini, P. Vázquez-Villegas, M. Rito-Palomares, S.O. Martinez-Chapa, Advantages, disadvantages and modifications of conventional ELISA, in: Enzyme-Linked Immunosorbent Assay ELISA, Springer Singapore, Singapore, 2018, pp. 67–115, 10.1007/978-981-10-6766-2_5.
[33] T. Todenhöfer, J. Hennenlotter, R. Ritter, U. Hoffmann, P. Blutbacher, A. Deja, A. Hohneder, A. Stenzl, C. Schwentner, 365 Point-of-care testing for bladder cancer – the UBC Rapid test on the concile® Ω100 reader platform provides quantitative results, Eur. Urol. Suppl. 12 (2013) e365.
[34] J.E. Lester, J.E. Brown, R.A. Hannon, S.P. Ellis, J.M. Horsman, O.P. Purohit, R. E. Coleman, The use of a point of care device for monitoring the bone resorption biomarker urinary N-telopeptide in cancer patients with bone metastases, Bone 46 (2010) 801–805, https://doi.org/10.1016/j.bone.2009.11.016.
[35] D. Kirby, M. Glynn, G. Kijanka, J. Ducrée, Rapid and cost-efficient enumeration of rare cancer cells from whole blood by low-loss centrifugo-magnetophoretic purification under stopped-flow conditions, Cytometry Part A 87 (2015) 74–80, https://doi.org/10.1002/cyto.a.22588.
[36] D. Issadore, Point-of-care rare cell cancer diagnostics, in: A. Rasooly, K.E. Herold (Eds.), Mob. Health Technol, Springer, New York, NY, 2015, pp. 123–137, https://doi.org/10.1007/978-1-4939-2172-0_9.
[37] A.S. Crawley, R.J. O'Kennedy, The need for effective pancreatic cancer detection and management: a biomarker-based strategy, Expert Rev, Mol. Diagn. 15 (2015) 1339–1353, https://doi.org/10.1586/14737159.2015.1083862.
[38] M. Oliveira-Rodríguez, S. López-Cobo, H.T. Reyburn, A. Costa-García, S. López-Martín, M. Yáñez-Mó, E. Cernuda-Morollón, A. Paschen, M. Valés-Gómez, M. C. Blanco-López, Development of a rapid lateral flow immunoassay test for detection of exosomes previously enriched from cell culture medium and body fluids, J. Extracell. Vesicles 5 (2016) 31803, https://doi.org/10.3402/jev.v5.31803.
[39] G. Liu, X. Mao, J.A. Phillips, H. Xu, W. Tan, L. Zeng, Aptamer−Nanoparticle Strip Biosensor for Sensitive Detection of Cancer Cells, Anal. Chem. 81 (2009) 10013–10018, https://doi.org/10.1021/ac901889s.
[40] A. Chamorro-Garcia, A. De La Escosura-Muñiz, M. Espinoza-Castañeda, C. J. Rodriguez-Hernandez, C. De Torres, A. Merkoçi, Detection of parathyroid hormone-like hormone in cancer cell cultures by gold nanoparticle-based lateral flow immunoassays, Nanomedicine Nanotechnol, Biol. Med. 12 (2016) 53–61, https://doi.org/10.1016/j.nano.2015.09.012.
[41] N.A. Taranova, A.E. Urusov, E.G. Sadykhov, A.V. Zherdev, B.B. Dzantiev, Bifunctional gold nanoparticles as an agglomeration-enhancing tool for highly sensitive lateral flow tests: a case study with procalcitonin, Microchim. Acta 184 (2017) 4189–4195, https://doi.org/10.1007/s00604-017-2355-4.
[42] P. Preechakasedkit, W. Siangproh, N. Khongchareonporn, N. Ngamrojanavanich, O. Chailapakul, Development of an automated wax-printed paper-based lateral flow device for alpha-fetoprotein enzyme-linked immunosorbent assay, Biosens. Bioelectron. 102 (2018) 27–32, https://doi.org/10.1016/j.bios.2017.10.051.
[43] M.-J. Lee, V. Soum, S.-N. Lee, J.-H. Choi, J.-H. Shin, K. Shin, B.-K. Oh, Pumpless three-dimensional photo paper–based microfluidic analytical device for automatic detection of thioredoxin-1 using enzyme-linked immunosorbent assay, Anal. Bioanal. Chem. 414 (2022) 3219–3230, https://doi.org/10.1007/s00216-021-03747-0.
[44] M. Kim, M.S. Kim, S.H. Kweon, S. Jeong, M.H. Kang, M.I. Kim, J. Lee, J. Doh, Simple and Sensitive Point-of-Care Bioassay System Based on Hierarchically Structured Enzyme-Mimetic Nanoparticles, Adv. Healthc. Mater. 4 (2015) 1311–1316, https://doi.org/10.1002/adhm.201500173.
[45] J. Zhang, L. Tang, Q. Yu, W. Qiu, K. Li, L. Cheng, T. Zhang, L. Qian, X. Zhang, G. Liu, Gold-platinum nanoflowers as colored and catalytic labels for ultrasensitive lateral flow MicroRNA-21 assay, Sens. Actuators B Chem. 344 (2021) 130325, https://doi.org/10.1016/j.snb.2021.130325.
[46] X. Mao, Y. Ma, A. Zhang, L. Zhang, L. Zeng, G. Liu, Disposable Nucleic Acid Biosensors Based on Gold Nanoparticle Probes and Lateral Flow Strip, Anal. Chem. 81 (2009) 1660–1668, https://doi.org/10.1021/ac8024653.
[47] W. Qiu, H. Xu, S. Takalkar, A.S. Gurung, B. Liu, Y. Zheng, Z. Guo, M. Baloda, K. Baryeh, G. Liu, Carbon nanotube-based lateral flow biosensor for sensitive and rapid detection of DNA sequence, Biosens. Bioelectron. 64 (2015) 367–372, https://doi.org/10.1016/j.bios.2014.09.028.
[48] G. Ruiz, K. Tripathi, S. Okyem, J.D. Driskell, pH Impacts the Orientation of Antibody Adsorbed onto Gold Nanoparticles, Bioconjug. Chem. 30 (2019) 1182–1191, https://doi.org/10.1021/acs.bioconjchem.9b00123.
[49] M. Maddahfar, S. Wen, S.M. Hosseinpour Mashkani, L. Zhang, O. Shimoni, M. Stenzel, J. Zhou, B. Fazekas De St Groth, D. Jin, Stable and highly efficient antibody-nanoparticles conjugation, Bioconjug. Chem. 32 (2021) 1146–1155, https://doi.org/10.1021/acs.bioconjchem.1c00192.
[50] A. Albanese, W.C.W. Chan, Effect of gold nanoparticle aggregation on cell uptake and toxicity, ACS Nano 5 (2011) 5478–5489, https://doi.org/10.1021/nn2007496.
[51] G. Wang, W. Sun, Optical limiting of gold nanoparticle aggregates induced by electrolytes, J. Phys. Chem. B 110 (2006) 20901–20905, https://doi.org/10.1021/jp0638843.
[52] C. Bee, Y.N. Abdiche, J. Pons, A. Rajpal, Determining the binding affinity of therapeutic monoclonal antibodies towards their native unpurified antigens in human serum, PLoS ONE 8 (2013) e80501.
[53] S.C. Devanaboyina, S.M. Lynch, R.J. Ober, S. Ram, D. Kim, A. Puig-Canto, S. Breen, S. Kasturirangan, S. Fowler, L. Peng, H. Zhong, L. Jermutus, H. Wu, C. Webster, E. S. Ward, C. Gao, The effect of pH dependence of antibody-antigen interactions on subcellular trafficking dynamics, mAbs 5 (2013) 851–859, https://doi.org/10.4161/mabs.26389.
[54] D. Goldblatt, L. Van Etten, F.J. Van Milligen, R.C. Aalberse, M.W. Turner, The role of pH in modified ELISA procedures used for the estimation of functional antibody affinity, J. Immunol. Methods 166 (1993) 281–285, https://doi.org/10.1016/0022-1759(93)90369-I.
[55] F. Poggialini, S. Legnaioli, B. Campanella, B. Cocciaro, G. Lorenzetti, S. Raneri, V. Palleschi, Calculating the Limits of Detection in Laser-Induced Breakdown Spectroscopy: Not as Easy as It Might Seem, Appl. Sci. 13 (2023) 3642, https://doi.org/10.3390/app13063642.

[56] U. Visentini, G. Cristoforetti, S. Legnaioli, A. Salvetti, E. Tognoni, V. Palleschi, Accurate measurement of magnesium content in alpha-olefins by laser induced breakdown spectroscopy (LIBS) technique, Optoelectron. Lett. 3 (2007) 222–226, https://doi.org/10.1007/s11801-007-6196-y.

[57] Survival Rates for Breast Cancer, (No uploaded date). https://www.cancer.org/cancer/types/breast-cancer/understanding-a-breast-cancer-diagnosis/breast-cancer-survival-rates.html (accessed January 10, 2024).

[58] GHTF Study Group 5 - Clinical Safety/Performance | International Medical Device Regulators Forum, (November 2, 2012). https://www.imdrf.org/documents/ghtf-final-documents/ghtf-study-group-5-clinical-safetyperformance (accessed January 10, 2024).

[59] National Comprehensive Cancer Network. NCCN clinical practice guidelines in oncology: Breast Cancer Screening and Diagnosis Ver. 1 2021, (May 6, 2021). http://www.nccn.org/professionals/physician_gls/pdf/breast.pdf. (accessed January 10, 2024).

[60] E.A. Sickles, Periodic mammographic follow-up of probably benign lesions: results in 3,184 consecutive cases, Radiology 179 (1991) 463–468, https://doi.org/10.1148/radiology.179.2.2014293.

[61] F02 Committee, Guide for Accelerated Aging of Sterile Barrier Systems for Medical Devices, (2021). https://doi.org/10.1520/F1980-21.